

# Displacive ion movements induced by localised surface plasmon resonance

*Masanori Sakamoto<sup>1</sup>\*, Masaki Hada<sup>2</sup>, Wataru Ota<sup>3,4</sup>, Fumihiko Uesugi<sup>5</sup>, & Tohru Sato<sup>3,4</sup>*

<sup>1</sup> Institute for Chemical Research, Kyoto University, Uji, Kyoto 611-0011, Japan.

<sup>2</sup> Tsukuba Research Center for Energy Materials Science (TREMS), Faculty of Pure and Applied Sciences, University of Tsukuba, 1-1-1 Tennodai, Tsukuba 305-8573, Japan

<sup>3</sup> Fukui Institute for Fundamental Chemistry, Kyoto University, Sakyo-ku, Kyoto 606-8103, Japan.

<sup>4</sup> Department of Molecular Engineering, Graduate School of Engineering, Kyoto University, Nishikyo-ku, Kyoto 615-8510, Japan.

<sup>5</sup> National Institute for Materials Science (NIMS), 1-1 Namiki, Tsukuba, Ibaraki 305-0044, Japan

E-mail: sakamoto@scl.kyoto-u.ac.jp

## **ABSTRACT (Summary Paragraph)**

The Jahn–Teller effect, a phase transition phenomenon involving spontaneous breakdown of symmetry in molecules and crystals, causes important physical and chemical changes that impact various fields of science, from the natural photosystem II to superconductors. In this study, we discovered that localised surface plasmon resonance (LSPR) induced the cooperative Jahn–Teller effect in covellite CuS nanocrystals (NCs), causing metastable displacive ion movements. Although light–matter interaction of plasmonic metal NCs has been widely investigated, the scope has been limited to collective mode stimulation. Electron diffraction measurements under photo illumination, ultrafast time-resolved electron diffraction analyses, and theoretical calculations of semiconductive plasmonic CuS NCs showed that metastable displacive ion movements due to the LSPR-induced cooperative Jahn–Teller effect caused a delay in the relaxation of LSPR in the microsecond region. Furthermore, the displacive ion movements caused photo-switching of conductivity in CuS NCs films used in room temperature ranges such as in transparent variable resistance infrared sensors. This study pushes the limits of plasmonics from the increase in tentative collective oscillation to metastable crystal structure manipulation, thereby expanding on Faraday's discovery.

## **MAIN TEXT**

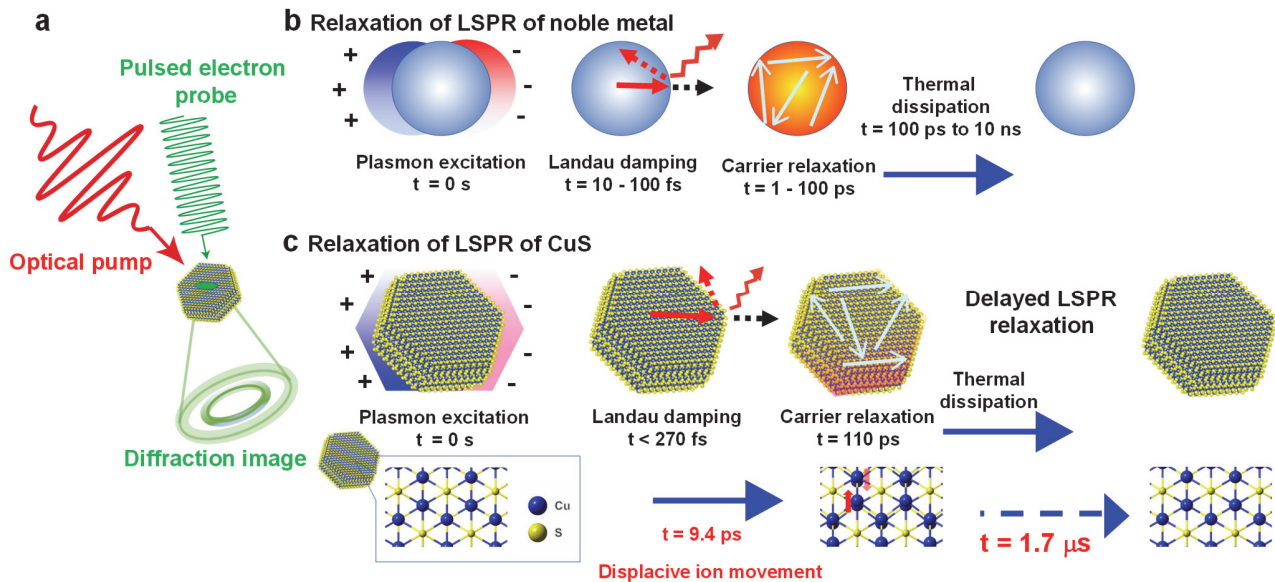
The science of localised surface plasmon resonance (LSPR), introduced by Faraday in 1857, is relevant across numerous scientific and industrial fields such as in device applications, energy conversion, catalysis, and so on.<sup>1–6</sup> LSPR is a collective oscillation of free carriers, and has been an important method to stimulate light–matter interactions by controlling the states of matter by changing properties and functions.<sup>7,8</sup> The light-to-matter interaction in LSPR of conventional noble metal nanocrystals (NCs) has been limited to the stimulation of the collective mode.<sup>9–11</sup> The collective oscillation of free carriers in LSPR leads to the stimulation of the phonon mode. The electron and phonon modes induced by LSPR are momentarily relaxed and less likely to lead to changes in the fundamental properties of the quantised

material due to light. Achieving LSPR-induced stimulation of the metastable atom/ion displacement, accompanied with a dramatic change in material properties, will push the limits of plasmonics.

Plasmonic semiconductors may exhibit different properties than the conventional plasmonic metals because of a moderately discretised band structure.<sup>12,13</sup> CuS NCs, an LSPR material, has been extensively investigated,<sup>13-17</sup> while its relaxation mechanism remains unclear. The relaxation of CuS NCs has been considered to be similar to that of metallic LSPR materials (such as noble metals); however, the semiconductive aspect is significant. Ludwig et al. used X-ray transient absorption spectroscopy to report that, unlike metal NCs with a continuous band structure, CuS NCs exhibits a carrier-trapping process, peculiar to semiconductors, in the ps region after LSPR excitation.<sup>18</sup> In addition to the general LSPR relaxation processes defining the above-mentioned consensus in LSPR relaxation, CuS NCs exhibits an inherently slow LSPR relaxation in the microsecond region (lifetime = 1.7  $\mu$ s).<sup>14</sup> This unique delay in relaxation is indicated by the laser flash photolysis results of CuS NCs as an extraordinary slow LSPR-bleach recovery. However, the origin has remained elusive because the spectroscopy data cannot directly track the ionic coordination in solids.

In this study, ultrafast time-resolved electron diffraction measurements with sub-picosecond time-resolution indicated that displacive ion movements by LSPR caused a delayed LSPR relaxation of CuS NCs (Scheme 1). Theoretical calculations predicted an LSPR-induced cooperative Jahn–Teller (JT) effect. The LSPR stimulated interaction between localised orbital electronic state and crystal lattice causes a phase transition (i.e. cooperative JT effect)<sup>19,20</sup> allowing ionic displacement in CuS NC. The conductivity of a CuS NCs film decreased upon LSPR excitation, following the LSPR-induced JT distortion. Based on the obtained results, we demonstrated the infrared (IR) responsive variable resistance of CuS film using the LSPR-induced JT distortion at room temperature. CuS NCs, which transmit visible light, look transparent.<sup>12</sup> The CuS NCs transparent film would be applicable for room temperature-driven optical IR sensors with the advantage of transparency, fast response, and printability. Although the LSPR relaxation process, linked to the phonon mode, causes a thermal lattice expansion (also called breathing/extensional mode),<sup>21-23</sup> there are no reports of metastable lattice rearrangement induced by LSPR. The plasmonic

control of metastable atomic configuration expands the scope of plasmonics, which could facilitate an in-depth understanding of the fundamental relationship between the atomic configuration and essential properties of the substance, as well as its potential applications.<sup>24-27</sup>



**Scheme 1. LSPR relaxation of CuS NCs.** **a)** Schematic representation of ultrafast electron diffraction used before optical-pump and electron diffraction probe experiments on colloidal nanocrystals (NCs) deposited on the substrate. **b)** Typical relaxation process of LSPR.<sup>3</sup> LSPR involves the coherent oscillation of free carriers stimulated by light.<sup>3,28</sup> Its relaxation process proceeds through Landau damping, electron-electron scattering, electron-lattice scattering, and lattice-lattice scattering, corresponding to time domains of 10–100 fs, 1–100 ps, and 0.1–100 ns, respectively.<sup>3,29</sup> **c)** LSPR relaxation process of CuS proceeds through Landau damping, carrier relaxation, and an unknown delayed relaxation corresponding to the time domains of < 270 fs, 110 ps, and 1.7  $\mu\text{s}$ , respectively.<sup>14</sup> The ionic displacements associated with LSPR excitation cause the delayed LSPR relaxation shown in the subsequent figures.

### Synthesis and characterisation of CuS NCs

CuS NCs were synthesised according to a previous publication.<sup>14</sup> Figure 1a shows transmission electron microscopy (TEM) images of CuS NCs (size:  $16.3 \pm 1.5 \text{ nm}$ , thickness:  $5.7 \pm 1.1 \text{ nm}$ ). The X-ray

diffraction (XRD) patterns show that the obtained NCs were composed of hexagonal covellite CuS (Inorganic Crystal Structure Database [ICSD] no. 26968) phases (Figure S1).

The elementary cell of CuS exhibits hexagonal symmetry corresponding to a  $P6_3/mmc$  space group with six formula units per unit cell (Figure 1b).<sup>30</sup> The atomic configuration of CuS consisted of three alternating layers (CuS<sub>4</sub>-tetrahedra layer/CuS<sub>3</sub>-triangles layer/CuS<sub>4</sub>-tetrahedra layer), where the CuS<sub>4</sub>-tetrahedra layers pinched the CuS<sub>3</sub>-triangles layers. In the CuS<sub>4</sub>-tetrahedra and CuS<sub>3</sub>-triangles, Cu ions exhibited tetrahedral coordination ( $Cu_{T_d}$ ) and trigonal coordination ( $Cu_T$ ), respectively. The three sulphur atoms of a CuS<sub>3</sub>-triangle, with one atom shared with a CuS<sub>4</sub>-tetrahedron, were labelled S(1) (Figure 1b), while the other sulphur atoms of the CuS<sub>4</sub>-tetrahedron were labelled S(2). The set of three alternating layers (CuS<sub>4</sub>-tetrahedra layer/CuS<sub>3</sub>-triangles layer/CuS<sub>4</sub>-tetrahedra layer) were connected along the *c*-axis via S(2)-S(2) bonds.

The calculated band structure of CuS is shown in Figure 1c. At the Fermi level, the electronic states consisted of mixed valence states of copper. Holes were elastically scattered among the degenerate orbitals at the Fermi level, making them free from Cu-atom charges. This imparted a p-type semiconducting behaviour to CuS NCs, which consequently exhibited an LSPR peak at 1080 nm (Figure 1d).

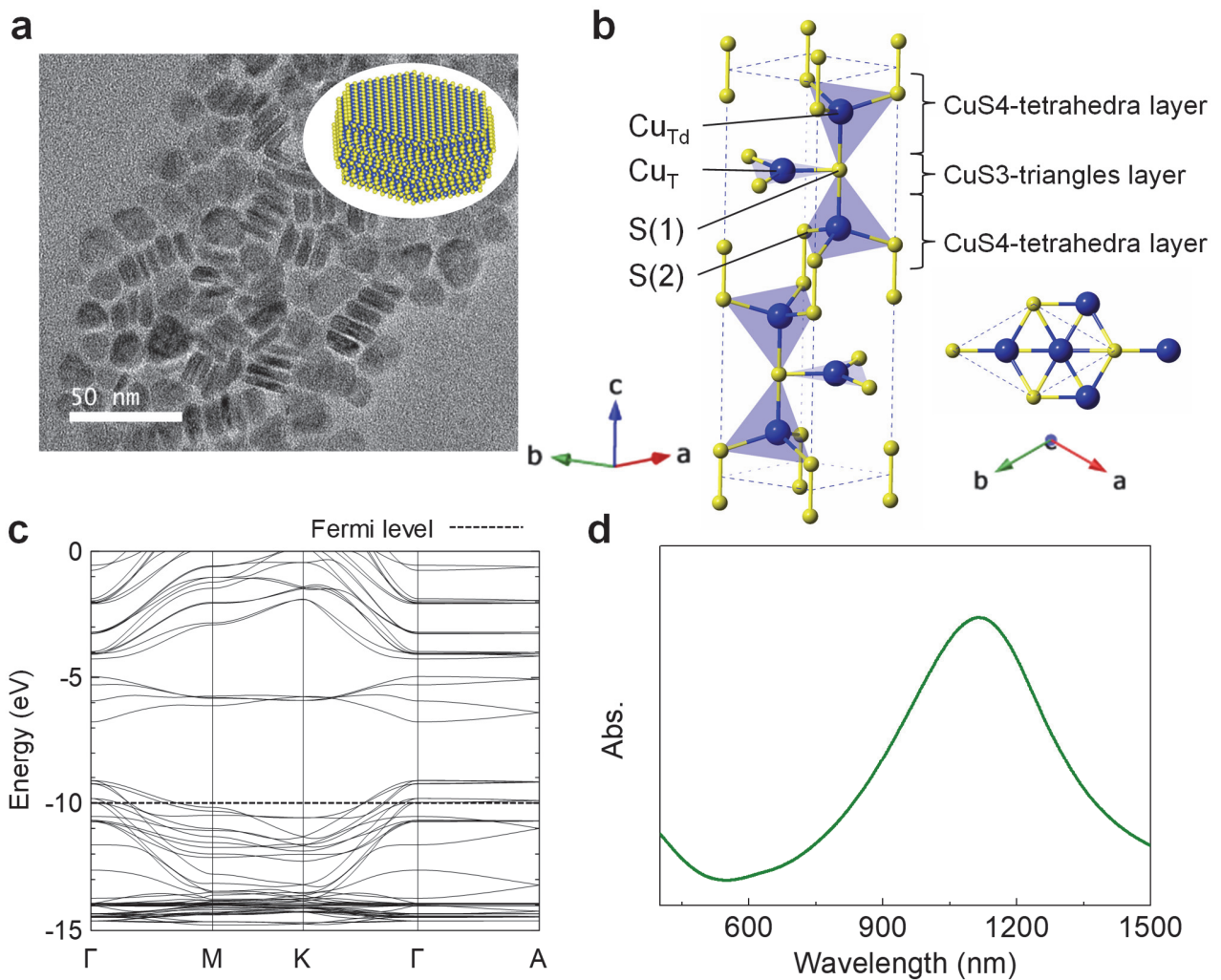


**Figure 1. Crystal structure and optical properties of the CuS NCs.** **a)** TEM image of the CuS NCs. **b)** Crystal unit cells of CuS with lattice constants of  $a = b = 3.796$  and  $c = 16.360$  Å. The yellow and blue spheres indicate sulphur and copper atoms, respectively. **c)** Calculated band structure of CuS within the tight-binding approximation (see Method section for details). **d)** UV–Vis–NIR absorption spectra of the CuS NCs in a chloroform dispersion.

### LSPR-induced atomic displacement of CuS NCs

The electron diffraction-pattern shift on light irradiation was directly observed to understand the LSPR relaxation process of a CuS NC from the viewpoint of the crystal structure (Figure 2). Without light

irradiation, the diffraction spots  $1\bar{3}0$  and  $2\bar{3}0$  of the CuS NCs exhibited an almost similar intensity, with a slight difference caused by the tilting of the NC against the vertical of the incident electron beam. Under light irradiation, the  $1\bar{3}0$  diffraction spot exhibited a higher intensity than the  $2\bar{3}0$  spot, while the  $130$  spot exhibited a lower intensity than the  $230$  spot. The simulation of crystal structures exhibiting the diffraction-spot shift indicated a movement of CuT (indicated by a red arrow in Figure 2c; see Figure S2–S4), which was validated by theoretical calculations (vide infra). The shift in the electron diffraction pattern indicated that the atomic displacement was a global phenomenon in the NCs.

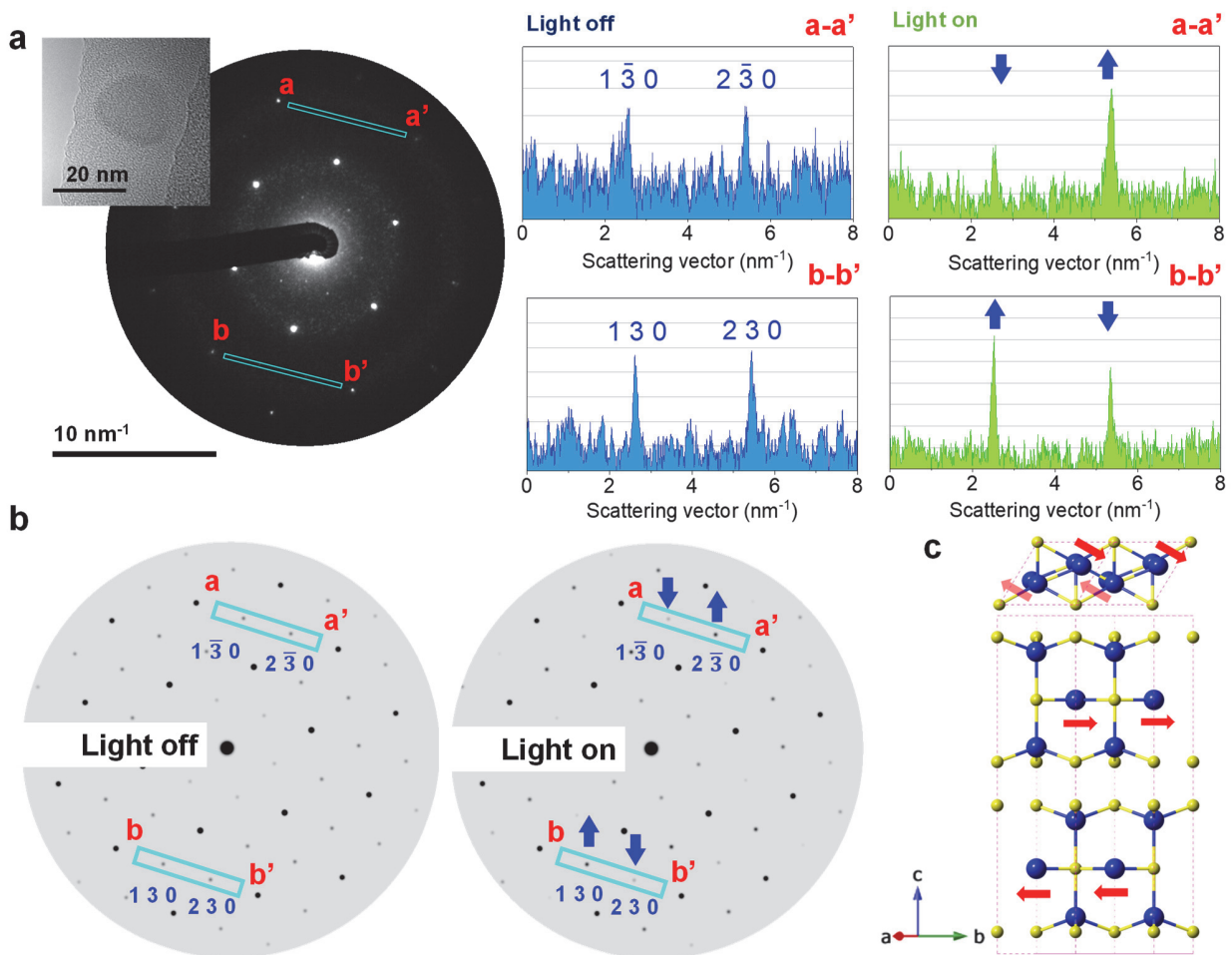


**Figure 2. Light-stimulated shift of the CuS NCs electron diffraction and its simulation.** **a)** Electron diffraction pattern of CuS under light irradiation. Inset: TEM image of CuS NCs corresponding to the electron diffraction pattern. The intensities of the diffraction peak in the blue rectangular region with and without light irradiation are shown on the right-hand side. The blue arrow indicates the intensity shift of the coupled diffraction spots ( $1\bar{3}0$  against  $2\bar{3}0$  and  $130$  against  $230$ ) under light irradiation. **b)** Simulated electron diffraction patterns of CuS NC with and without light irradiation. **c)**  $Cu_T$  shifts causing an electron diffraction pattern corresponding to the ionic motion indicated by the red arrows (see the Supplementary Information for details).

### Time-resolved electron diffraction measurement

Ultrafast time-resolved electron diffraction measurements were used to investigate the lattice relaxation of CuS NCs after LSPR excitation.<sup>24,26,31</sup> The electron diffraction pattern of the 60-nm-thick CuS NCs film indicated two rings on the (012) and (110) planes, as shown in Figure 3a, owing to the NCs being randomly oriented in the lateral direction and highly oriented (more than 70%) along the [001] axis (in the longitudinal direction). The  $110$  diffraction ring was more intense than the  $012$  diffraction ring (Figure 3a); therefore, the peak intensities and positions (scattering vector:  $Q = 1/d$ , where  $d$  is the lattice spacing) were analysed from the  $110$  diffraction ring.

The time evolution of the intensity and peak-position of the diffraction ring after irradiation with 400- and 800-nm light with an incident fluence of  $5 \text{ mJ cm}^{-2}$  is shown in Figure 2b and 2c, respectively. The 400- and 800-nm light induced bandgap excitation and LSPR excitation, are also shown in these figures. Below an incident fluence of approximately  $8 \text{ mJ cm}^{-2}$ , the photoexcitation phenomenon occurred in a repetitive regime. Light excitation (via 400- and 800-nm light) caused a negative shift of the  $Q$ -value of the (110) plane (Figure 2b), indicating a lattice expansion of the CuS NCs by laser heating. Owing to the size effect of nanocrystals, the CuS lattice could expand on a slight temperature rise. As shown in Figure

2c, excitation of the LSPR band using an 800-nm laser changed the intensity of the 1 1 0 diffraction ring; this differed from bandgap excitation. The intensity of the 1 1 0 diffraction ring decreased by ~6% with a  $9.4 \pm 3.1$  ps excitation of the LSPR band. Almost half of the intensity shift (~3%) was recovered, with a time constant of  $45 \pm 16$  ps, while the other half remained low, and no temporal shift was observed within the time window provided by the instrument used. This could indicate a large lattice expansion immediately after LSPR excitation, subsequently transforming into a metastable crystal structure. This result agrees with the TEM observation of a shift in the diffraction spot under light irradiation.

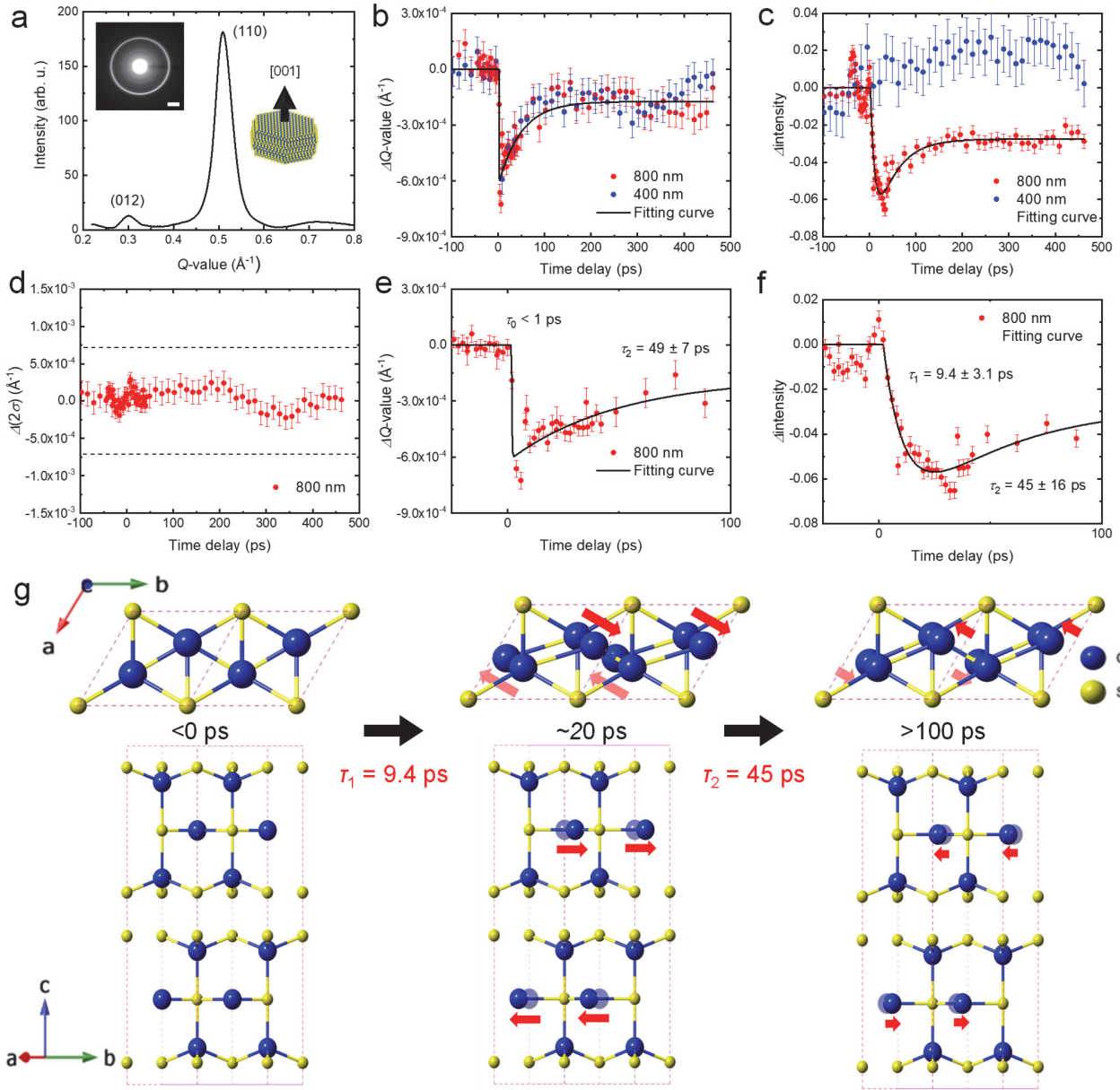


**Figure 2. Time-resolved electron diffraction of the CuS NCs.** **a)** Radially-integrated diffraction intensity of the CuS NCs film. Inset: Electron diffraction pattern. The white scale bar represents  $0.2 \text{ \AA}^{-1}$ .

**b)** Time evolution of the  $Q$ -value from the (110) planes under fs-laser excitation in the wavelength range of 400–800 nm.

**c)** Time evolution of the electron diffraction intensity from the (110) planes under fs-laser excitation in the wavelength range of 400–800 nm.

**d)** Temporal shift in the FWHM of the electron diffraction intensity from the (110) planes under fs-laser excitation at 800 nm. The blue dotted lines indicate the peak shifts derived from **b**.

**e)** Magnified time evolution of the  $Q$ -value obtained from the data in **b**. The time delay is shown from 0 to 100 ps, with  $\tau_0 < 1 \text{ ps}$ ,  $\tau_2 = 49 \pm 7 \text{ ps}$ , and  $\tau_1 = 9.4 \pm 3.1 \text{ ps}$ .

**f)** Magnified time evolution of the intensity obtained from the data in **c**. The time delay is shown from 0 to 100 ps, with  $\tau_1 = 9.4 \pm 3.1 \text{ ps}$ ,  $\tau_2 = 45 \pm 16 \text{ ps}$ , and  $\tau_0 < 1 \text{ ps}$ .

**g)** Schematic diagram showing the CuS lattice structure at three time delays: <0 ps,  $\sim 20 \text{ ps}$ , and >100 ps. The Cu atoms are represented by blue spheres and the S atoms by yellow spheres. Red arrows indicate the movement of Cu atoms between layers. The axes are labeled a, b, and c.

(110) electron diffraction rings under fs-laser excitation at 800 nm. The solid black line indicates the best fit. **f)** Magnified time evolution of the electron diffraction intensity from the (110) planes under fs-laser excitation at 800 nm. The solid black line indicates the best fit. **g)** Time-resolved illustration of the light-stimulated ionic displacement occurring in CuS NCs.

Intensity changes in diffraction rings are caused by atomic movements in a unit cell or the Debye-Waller effect.<sup>32</sup> As shown in the Supplementary Information (Figure S5), laser heating with 800-nm light caused a temperature increase in the range of 11 K. This can induce modulation of less than 1% in diffraction intensity.<sup>32</sup> Thus, the photo-induced intensity changes in the diffraction pattern of the CuS NCs could not be attributed to the simple photo-thermal Debye-Waller effect. The decrease in diffraction intensity, which was not observed in bandgap excitation (under 400-nm light), indicated that LSPR excitation (under 800-nm light) induced ionic displacements in the unit cell without a change in the long-range structural periodicity.

Diffraction intensity shifts reflect local or cooperative ionic displacements; thus, the temporal shift of the half-width ( $2\sigma$ ) of the diffraction peak was investigated. As an inhomogeneous distortion in NCs induces width broadening, a local ionic displacement should increase width. However, as shown in Figure 2d, the diffraction width did not shift significantly after LSPR excitation, indicating that the observed ionic displacement was a cooperative phenomenon. Thus, LSPR excitation changed the crystal structure of the NCs to a metastable state.

To further discuss the LSPR-induced ionic displacement in CuS NCs, the time evolution of the intensity and peak-position of the diffraction ring immediately after LSPR excitation (Figures 2e and 2f) was investigated. A shift in the  $Q$ -value occurred within the pulse duration of the probe electron pulse (< 1 ps), and the time constant indicated that this rapid shift corresponded to the laser heating-mediated lattice expansion observed in LSPR materials.<sup>22,23</sup> In contrast to the  $Q$ -value shift, the intensity of the 1 1 0

diffraction ring gradually shifted after laser excitation, exhibiting a time constant of  $9.4 \pm 3.1$  ps. Subsequently, the shift was recovered with a time constant of  $45 \pm 16$  ps, indicating stabilisation to a metastable state. The time constant indicated that the displacive ion movements occurred in the carrier- or carrier-phonon-scattering stage during LSPR relaxation.

## Theoretical calculations

Theoretical calculations within the tight-binding approximation<sup>32</sup> were used to qualitatively analyse the electronic structures of CuS that caused the experimentally observed Cu<sub>T</sub> movement under 800-nm light excitation. The time-resolved electron diffraction measurements under light irradiation showed that the ions moved in the same direction in each unit cell (Figure 2c), suggesting that the 800-nm light caused electronic transitions at the  $\Gamma$  point. An enlarged view of the band structure around the  $\Gamma$  point (Figure S6a) showed that the lowest unoccupied crystal orbital (LUCO) is degenerate at the  $\Gamma$  point. The electron excitation to the degenerate LUCO from the lower-energy orbitals at the  $\Gamma$  point induced the JT effect. One of the degenerate LUCOs has bonding and the other anti-bonding characteristics between the Cu<sub>T</sub>-S(1) bond (Figure S6b). Therefore, the excitation of the LUCOs generated ionic displacements, shortening the Cu<sub>T</sub>-S(1) bond. The planar triangle consisting of Cu<sub>T</sub> and three S(1), where the LUCOs are distributed, has  $D_{3h}$  site symmetry. Thus, the irreducible representation of the degenerate excited state localised around this site is considered to be  $E'$  or  $E''$ . Their symmetrical product is  $[E'^2] = [E''^2] = A'_1 \oplus E'$ , indicating that the degenerate excited electronic state couples with a vibrational mode (with representation  $e'$ ) to give the  $E \otimes e$  problem. The epikernel of  $e'$  in the parent group  $D_{3h}$  is  $C_{2v}$ .<sup>33</sup>

$$E(D_{3h}, e') = C_{2v}.$$

Therefore, according to the epikernel principle,<sup>33</sup> the JT effect lowers the site symmetry of the planar triangle to  $C_{2v}$ . Thus, the excitation of the degenerate LUCO at the  $\Gamma$  point induced the  $E \otimes e$  JT effect, lowering the site symmetry around Cu<sub>T</sub> from  $D_{3h}$  to  $C_{2v}$  thus shortening the Cu<sub>T</sub>-S(1) bond. These results

are in agreement with ion movements predicted by the time-resolved electron diffraction measurements. During the shift of the 1 1 0 diffraction ring upon LSPR excitation (around 7%), the CuT moved ~0.19 Å (9.5 ps after LSPR excitation). Subsequently, the ionic-displacement shift of CuT settled into a metastable state with a 0.165 Å CuT shift and a time constant of 45 ps.

## Device application

To analyse the LSPR-induced displacive ion movement as a macroscopic phenomenon, the LSPR-responsive photoconductivity of the CuS NCs film was investigated (Figure 3). A thin film of CuS NCs (thickness: 50 nm) was prepared on a comb electrode using the layer-by-layer deposition method (see Method section for details). The CuS NCs film was set on a temperature controller with a heat sink and a Peltier element to avoid any thermal effect of infrared irradiation on its conductivity. IR-light irradiation caused a decrease in its conductivity (Figure 3b). The CuS film showed semiconductive behaviour in temperature-dependent conductivity measurements, thus, an increase in temperature via IR light should not decrease the conductivity of the film (see Figure S7). Additionally, a shift in the conductivity ratio against photon flux reproduced the LSPR peak of CuS (Figure 3c). Therefore, the decrease in conductivity by IR irradiation could be attributed to the change in crystal structure induced by LSPR. The LSPR of CuS NCs underwent a redshift under IR-light irradiation.<sup>14</sup> The redshift indicated that the number of free carriers contributing to the conductivity decreased under IR-light irradiation. The shift of LSPR validated this result under IR-light irradiation.<sup>14</sup> The CuS transparent film would be applicable for room temperature-driven optical IR sensors. The advantages of transparency, fast response, and printability of the CuS films are favourable for invisible wearable IR sensing devices and/or neural sensing, among others.<sup>34,35</sup>

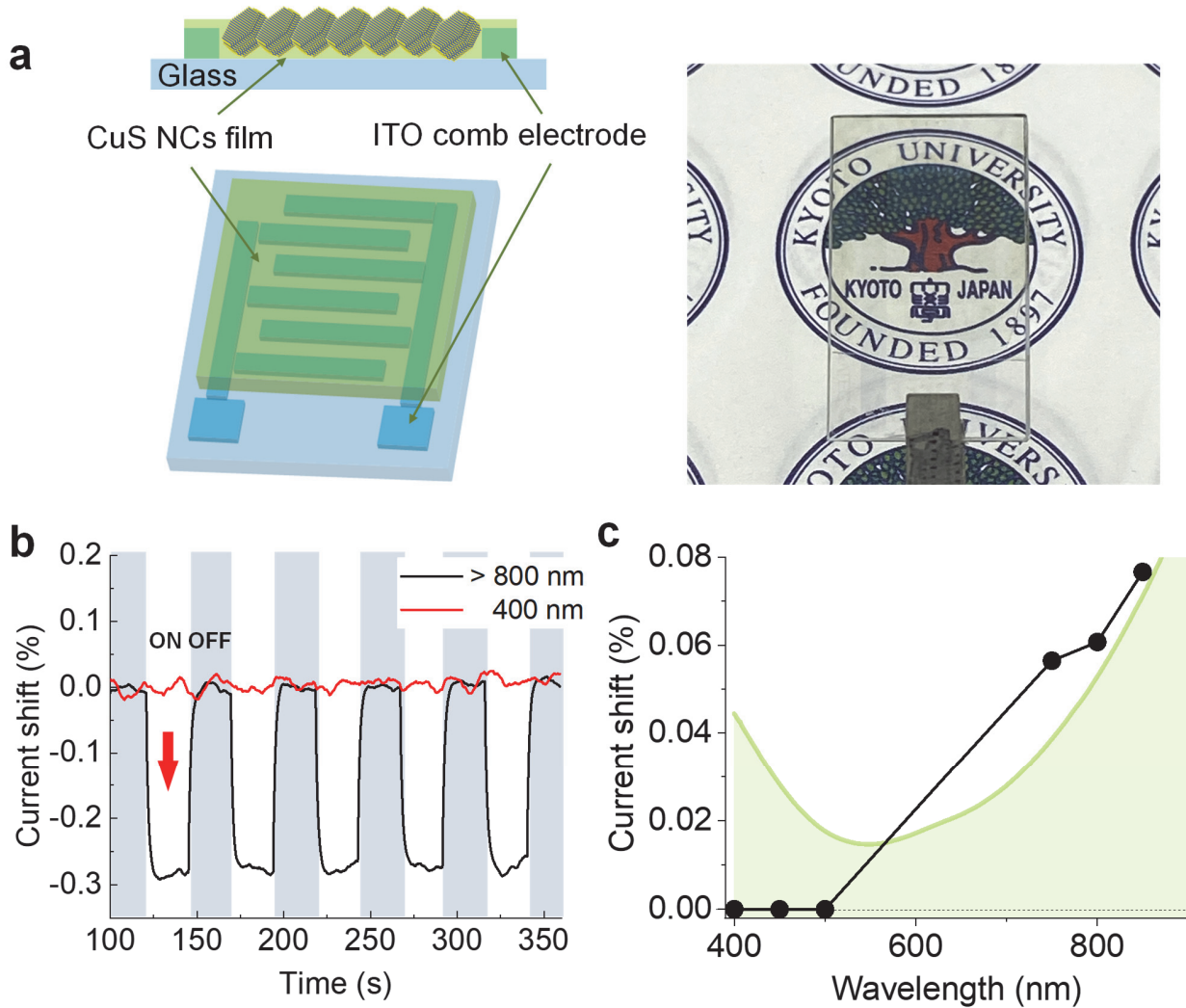


**Figure 3. Device application of the light-stimulated ionic displacement in CuS NCs.** **a)** Illustrations of devices (left-hand image). Photograph of a CuS NCs film coated on an ITO comb electrode (right-hand image). **b)** IR light ( $> 800$  nm) responsive photoconductivity (central image) of the CuS NCs film with a voltage of +1 V. **c)** Excitation wavelength dependent on photoconductivity shift of the CuS NCs film with a voltage of +1 V. The green line indicates the extinction spectra of CuS, indicating that a shift in resistance occurs in response to LSPR.

## Discussion

The entire LSPR relaxation process of CuS NCs, in chronological order, is shown in Scheme 1c. LSPR excitation stimulated lattice expansion by laser heating within 1 ps, which induced the phonon mode (correlated to the expansion coordinate of the NC) and caused inter-band transitions,<sup>36</sup> stimulating the JT mode. The stimulated JT mode caused displacive ionic movements of Cu<sub>T</sub> in ~10 ps. The strain induced by the cooperative JT effect induced an LSPR redshift and a decrease in conductivity. The twist in the crystal structure (i.e., atomic displacement) was released after eliminating the JT distortion, indicated by the delayed relaxation of LSPR.

Lindenberg et al. have reported that localised carrier trapping, which forms the surface polarons in quantum dots (QDs),<sup>26</sup> also induced lattice distortion. However, the phenomenon exhibited in this study was not because of carrier-trapping distortion but the cooperative JT distortion of the NCs. Lattice distortion in a semiconductor QD by bandgap excitation is localised and not cooperative,<sup>37</sup> whereas LSPR-induced hot-carrier generation is comprehensive, as indicated by the width shift and electron diffraction under light irradiation.

## Conclusion

The LSPR-induced cooperative JT effect described herein enabled a crystal structure shift with an extremely long lifetime due to the unique nature of the JT effect. The material design based on the vibronic coupling theory could be applicable for developing drastic and long-lived LSPR-induced ionic displacement with desired functional switching.<sup>38</sup> The combination of LSPR and the cooperative JT effect could guide the atomic-configuration manipulation of plasmonic nanomaterials in future research. The observations in this study could also be applicable for light stimulation of physical phenomena influenced by the cooperative JT effect, such as metal-insulator transition, superconductivity, and colossus magnetoresistance.<sup>7,39,40</sup> Furthermore, the LSPR-induced JT effect could provide an alternative to elucidate the interaction between functions and atomic configuration in NCs.

## References

- 1 Faraday, M. X. The Bakerian Lecture. 2014; Experimental relations of gold (and other metals) to light. *Philosophical Transactions of the Royal Society of London* **147**, 145-181 (1857).
- 2 Fusella, M. A. *et al.* *Nature* **585**, 379-382 (2020).
- 3 Brongersma, M. L., Halas, N. J. & Nordlander, P. *Nat. Nanotechnol.* **10**, 25-34 (2015).
- 4 Sytwu, K. *et al.* *Science* **371**, 280-283 (2021).
- 5 Naldoni, A., Shalaev, V. M. & Brongersma, M. L. *Science* **356**, 908-909 (2017).
- 6 Mueller, N. S. *et al.* *Nature* **583**, 780-784 (2020).
- 7 Bloch, J., Cavalleri, A., Galitski, V., Hafezi, M. & Rubio, A. *Nature* **606**, 41-48 (2022).
- 8 Basov, D. N., Averitt, R. D. & Hsieh, D. *Nat. Mater.* **16**, 1077-1088 (2017).
- 9 Lei, D. Y. *et al.* *ACS Photonics* **2**, 1306-1313 (2015).
- 10 Schumacher, L. *et al.* *J. Phys. Chem. C* **123**, 13181-13191 (2019).
- 11 Wang, Y. *et al.* *J. Am. Chem. Soc.* **144**, 3517-3526 (2022).
- 12 Sakamoto, M. *et al.* *Nat. Commun* **10**, 406 (2019).
- 13 Luther, J. M., Jain, P. K., Ewers, T. & Alivisatos, A. P. *Nat. Mater.* **10**, 361-366 (2011).
- 14 Lian, Z. *et al.* *Nature Commun.* **9**, 2314 (2018).
- 15 Goel, S., Chen, F. & Cai, W. *Small* **10**, 631-645 (2014).
- 16 Xie, Y. *et al.* *ACS Nano* **7**, 7352-7369 (2013).
- 17 Ma, G. *et al.* *ACS Nano* **7**, 9010-9018 (2013).
- 18 Ludwig, J. *et al.* *J. Phys. Chem. Lett.* **6**, 2671-2675 (2015).
- 19 Gehring, G. A. & Gehring, K. A. *Rep. Prog. Phys* **38**, 1-89 (1975).
- 20 Sato, T., Chibotaru, L. F. & Ceulemans, A. *J. Chem. Phys.* **122**, 054104 (2005).
- 21 Ligges, M. *et al.* *App. Phys. Lett.* **94**, 101910, (2009).
- 22 Devkota, T., Brown, B. S., Beane, G., Yu, K. & Hartland, G. V. *J. Chem. Phys.* **151**, 080901 (2019).
- 23 Hu, M. *et al.* *J. Am. Chem. Soc.* **125**, 14925-14933 (2003).
- 24 Hada, M., Nishina, Y. & Kato, T. *Acc. Chem. Res* **54**, 731-743 (2021).
- 25 Rini, M. *et al.* *Nature* **449**, 72-74 (2007).
- 26 Eichberger, M. *et al.* *Nature* **468**, 799-802 (2010).
- 27 Fiebig, M., Miyano, K., Tomioka, Y. & Tokura, Y. *Science* **280**, 1925-1928 (1998).
- 28 Link, S. & El-Sayed, M. A. *Annu Rev Phys Chem* **54**, 331-366 (2003).
- 29 Hartland, G. V. *Annu Rev Phys Chem* **57**, 403-430 (2006).
- 30 Ohmasa, M., Suzuki, M., Tak, Eacute & Uchi, Y. *Mineral. J.* **8**, 311-319 (1977).
- 31 Ishikawa, T. *et al.* *Science* **350** (2015).
- 32 Hada, M. *et al.* *J. Chem. Phys.* **145**, 024504 (2016).
- 33 Ceulemans, A. & Vanquickenborne, L. G. *Struct Bond* **71**, 125-159 (1989).
- 34 Li, Q., van de Groep, J., Wang, Y., Kik, P. G. & Brongersma, M. L. *Nat. Commun* **10**, 4982 (2019).
- 35 Park, D.-W. *et al.* *Nat. Protoc* **11**, 2201-2222 (2016).
- 36 Hartland, G. V., Besteiro, L. V., Johns, P. & Govorov, A. O. *ACS Energy Lett.* **2**, 1641-1653 (2017).
- 37 Guzelturk, B. *et al.* *Nat. Commun.* **12**, 1860 (2021).
- 38 Kato, T. H., N.; Sato, T. *Vibronic Coupling Density*. (Springer Nature, 2021).
- 39 Guzmán-Verri, G. G., Brierley, R. T. & Littlewood, P. B. *Nature* **576**, 429-432 (2019).
- 40 Fausti, D. *et al.* Light-Induced Superconductivity in a Stripe-Ordered Cuprate. *Science* **331**, 189-191 (2011).
- 41 Momma, K. & Izumi, F. *J. Appl. Crystallogr.* **44**, 1272-1276 (2011).

- 42 Hoffmann, R. An Extended Hückel Theory. I. Hydrocarbons. *J. Chem. Phys.* **39**, 1397-1412 (1963).
- 43 Landrum, G. G., W. *Yet Another Extended Hückel Molecular Orbital Package* (YAeHMOP) <<http://yaehmop.sourceforge.net>>
- 44 Ramirez, R. & Böhm, M. C. *Int. J. Quantum Chem.* **34**, 571-594 (1988).

## Method

### Synthesis of CuS NCs

Hexagonal plate-like CuS NCs were synthesised according to a previous publication.<sup>10</sup> A mixture of copper (I) acetate (0.123 g, 1 mmol) and oleylamine (10 mL) was degassed at 160 °C for 30 min. Subsequently, a solution of sulphur (0.048 g, 1.5 mmol) in 1-octadecene (15 mL) was injected rapidly into the mixture under a nitrogen atmosphere and stirred for 10 min. The resulting product was purified by adding an ethanol-hexane ( $v: v = 1: 1$ ) mixed solvent to the solution, by centrifuging twice, and then redispersing the precipitate in hexane.

### Characterisation

High-resolution transmission electron microscopy (HRTEM) characterisation was carried out using a JEM-2200FS (JEOL) electron microscope at an acceleration voltage of 200 kV. XRD patterns were recorded on a PANalytical Aeris diffractometer, with Cu K $\alpha$  radiation ( $\lambda = 1.542 \text{ \AA}$ ) at 40 kV and 15 mA. Ultraviolet-visible-near-infrared (UV–Vis–NIR) absorption spectra were recorded using a UV-3600 spectrophotometer (Shimadzu).

### Time-resolved electron diffraction measurements

Details of the ultrafast time-resolved electron diffraction setup are mentioned in another publication.<sup>22</sup> Ultrafast time-resolved electron diffraction produced ultrashort (~1 ps) electron pulses. A 75 keV electrostatic field accelerated the electron beam, and the repetition-rate of electron pulses was 1 kHz. The

CuS film (60~70 nm) on the ultrathin silicon nitride substrate was excited by near-UV and NIR pulses (wavelengths of 400 and 800 nm, respectively) synchronised with electron pulses. The fluence of the exciting pulses was set to 5 mJ cm<sup>-2</sup>.

### **Simulation of LSPR-induced atomic displacement**

Electron diffraction patterns were calculated using the CrystalMaker®, CrystalDiffract®, and SingleCrystal® software packages, based on kinematic theory. Covellite CuS, with the *P6<sub>3</sub>/mmc* space group, was used as the initial structure during analysis. The crystal structure and NC in the figures were made using VESTA®.<sup>41</sup> The atomic motions in CuS induced by photoexcitation were derived using theoretical calculations.

### **Theoretical calculations**

The electronic structures of CuS were computed using the extended Hückel theory<sup>42</sup> with the parameters provided in YAeHMOP.<sup>43</sup> The Brillouin zone was sampled with 405 *k*-points selected based on the method of Ramirez and Böhm.<sup>44</sup> The extended Hückel theory was employed instead of the density functional theory (DFT). This is because the DFT calculations of CuS resulted in a zero energy gap near the Fermi level,<sup>44</sup> although the 400-nm light is known to induce the bandgap excitation experimentally. The DFT+*U* calculations also yielded a significantly small energy gap (~0.2 eV) in comparison with the 400-nm light.<sup>44</sup> These indicate that DFT cannot reproduce the experimental observation. On the other hand, the extended Hückel theory well describes the band structure, consistent with the experiments.

### **Conductivity measurement of the CuS NCs film**

A CuS NCs film with a thickness of 60 nm was fabricated on Au and ITO comb electrodes using layer-by-layer deposition of octan solutions of CuS NCs and short ligands (0.3 % KSCN solution of methanol) via ligand exchange. A 300 W Xe lamp (Cermax, Excelitas Technology) equipped with a UV–Vis cutoff

filter ( $\lambda > 800$  nm, power density: 50 mW cm<sup>-2</sup>) was used as the light irradiation source. To avoid any thermal effect on conductivity, the electrode was set on a Peltier device during IR-light irradiation.

## Data availability

The data sets within this article and the Supplementary Information are available from the authors upon request.

## Acknowledgements

M.S. is grateful to Tetsuri Nishikawa, Hiroki Morishita, and Norikazu Mizuochi for Hall measurements, and M.H. is grateful to Shin Ueno and Wataru Yajima for experimental assistance. M.S. and M.H. are grateful to Satoshi Ohmura for fruitful discussions. This work was supported by the "Joint Usage/Research Program on Zero-Emission Energy Research" of the Institute of Advanced Energy, Kyoto University (ZE2020C-0), and JSPS KAKENHI Grant Numbers: JP22K05253 in Scientific Research (C) (T.S.), JP21H04638 in Scientific Research (A) (M.S.), JP20H01832 in Scientific Research (B) (M.H.), and JP20H04657 in Scientific Research on Innovative Areas (M.H.). This work was also supported by the JST FOREST Program (Grant Number PMJFR201M, JPMJFR211V) (M.S., M.H.) and the Adaptable and Seamless Technology transfer Program through Target-driven R&D (A-STEP): JST Grant Number JPMJTR20T1 (M.S.). Numerical calculations were carried out using the Supercomputer System of the Institute for Chemical Research, Kyoto University, Academic Center for Computing and Media Studies (ACCMS), Kyoto University, and the Research Centre for Computational Science, Okazaki (Project: 22-IMS-C065).

## Author contributions

M.S. conceived and designed the experiments and carried out material fabrication and device application. M.H. carried out the time-resolved electron diffraction measurement. F.U. carried out the electron diffraction measurement in TEM with and without light irradiation and simulation of atomic displacement.

T.S. and W.O. carried out theoretical calculations. M.S., M.H., T.S., and W.O. wrote the manuscript. All authors participated in the discussion of the research.

### **Competing interests**

The authors declare no competing interests.

### **Additional information**

#### ***Supplementary Information***

Supplementary Information is available for this paper.

#### ***Correspondence and requests for materials***

Correspondence and requests for materials should be addressed to M.S.